Rigidity of randomly intercalated layered solids

M. F. Thorpe, W. Jin, and S. D. Mahanti
Department of Physics and Astronomy and Center for Fundamental Materials Research, Michigan State University, East Lansing, Michigan 48824
(Received 2 June 1989)

We set up a harmonic spring model that describes both the layer rigidity and the size and stiffness of the intercalant species. In certain limiting cases, when (1) the layers are either perfectly floppy or perfectly rigid and (2) the stiffness of the two intercalant species are the same, the model can be solved exactly. We also give an effective-medium solution that reproduces all the known exact results, and agrees well with numerical simulations in other cases. These simulations are performed for both one- and two-dimensional systems. If the two intercalant species have the same spring constant, Vegard's law is recovered. We compute the probability distribution of the various interlayer distances and apply the results to two-dimensional alloys of Li and vacancies in graphite, and to K and Rb in graphite.

I. INTRODUCTION

All crystalline solid solutions show a composition dependence of the average unti-cell volume $\langle V \rangle$ which increases with the concentration of the largest constituent.[1] Simple examples of such systems are binary alloys of the type $A_{1-x}B_x$ in the quenched limit when the species A and B are randomly distributed, and ternary systems of the type $A_{1-x}B_xC$. The linear variation of $\langle V \rangle$ with x is the well-known Vegard's law,[2] although most solid solutions do exhibit a complex nonlinear (superlinear, sublinear, sigmoidal) behavior. The x dependence of $\langle V \rangle$ depends, at the microscopic level, on the competition between local and global energies associated with forming a solid solution. These energies depend upon the relative size and compressibility of the different atomic species and overall rigidity of the system.

To address the question of the x dependence of both the average volume $\langle V \rangle$ and fluctuations in the unit-cell volume from site to site, it is somewhat simpler theoretically to consider either systems of reduced dimensionality or those with large anisotropy in physical properties. For example, there is a considerable variety of ternary layered intercalated compounds of the form $A_{1-x}B_xL$, with $o \leq x \leq 1$ [where B (A) is the larger (smaller) intercalant, and L denotes the layer] where the major expansion takes place along the direction perpendicular to the layers, denoted as the c axis.[3–8]

In the past, several attempts have been made to study the nonlinear x dependence of the c-axis expansion within two quite distinct types of models. One is referred to as the rigid-layer model[4,9] in which the layers are assumed to be flat, i.e., perfectly rigid against transverse distortions. In this model the nonlinearity in the c-axis expansion arises from the finite but different compressibilities of the two intercalants A and B. The second is referred to as the layer-rigidity model,[9–12] in which the layers are assumed to be deformable but the intercalants are taken to be perfectly incompressible but having different sizes. This model has been solved in the case where there are only two allowed heights and gives a simple functional form that seems to fit the observed layer thickness well in some compounds such as Cs_x Rb_{1-x} vermiculite.[10,11] The second model has also been solved using an elastic continuum approximation[12,13] in the low-defect-concentration limit (i.e., x close to 0 or 1). Simultaneous inclusion of the effects of both the local ionic compressibility and the finite layer rigidity on the c-axis expansion has not been possible until the present time. In this paper, we rectify this shortcoming by studying in detail a model which incorporates both the above effects.

In Sec. II we introduce the spring model and in Sec. III we present results of exact calculations in certain limiting cases. In Sec. IV we develop an effective-medium theory and test its accuracy by comparing the results with the exact calculations. In Sec. V numerical simulations are compared with the effective-medium-theory results and finally in Sec. VI we make some general remarks and compare our simulation and effective-medium-theory results with available experiments in graphite intercalation compounds.

II. THE MODEL

Consider a layered ternary system with composition $A_{1-x}B_xL$, where L represents the host layer such as graphite, dichalcogenide, or vermiculite. A and B are two different types of intercalants which are assumed to occupy (randomly) a set of well-defined lattice sites (see Fig. 1). The total energy of the system can be approximated by a sum of two major contributions; one associated with the interaction between the intercalants and the host and the other between host atoms themselves. Since we assume the intercalants to be frozen (i.e., quenched), the direct interaction energy between the intercalants does not play any role in the layer distortion. In a real ternary which consists of many layers, the experimentally measured average interlayer spacing will, to some degree, depend on the interlayer correlation. The latter results from large intercalant ions in the adjacent galleries repel-

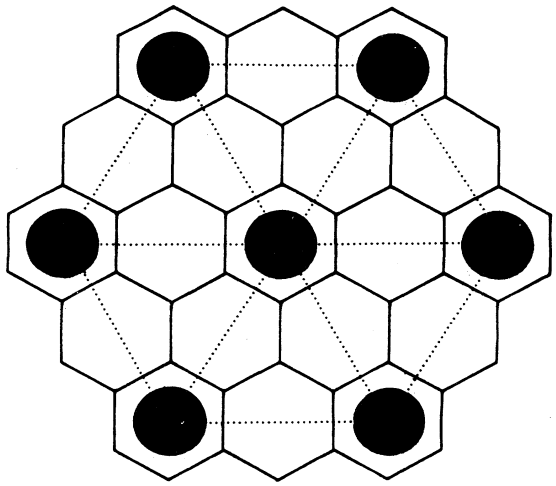

FIG. 1. Top view of a hexagonal lattice host layer where the intercalants form a triangular lattice.

ling each other,[9] and other similar effects. This effect is likely to be important in the limit of a small concentration x of the large ion. In the present paper, we neglect this correlation and consider a single gallery bounded by two host layers with intercalants randomly occupying lattice sites inside the gallery. It is possible that the interlayer correlation effects can be largely taken care of by a proper redefinition of spring constants.

The total energy of the host layer-intercalant system can be written as

$$E=\tfrac{1}{2}\sum_{\vec{i}}K_{\vec{i}}(h_{\vec{i}}-h^0_{\vec{i}})^2+\tfrac{1}{2}\sum_{\langle\vec{i},\vec{\delta}\rangle}K_T(h_{\vec{i}}-h_{\vec{i}+\vec{\delta}})^2 +\tfrac{1}{2}\sum_{\vec{i}}K_F\left[\sum_{\vec{\delta}}(h_{\vec{i}}-h_{\vec{i}+\vec{\delta}})\right]^2 , \tag{1}$$

where $h_{\vec{i}}$ is the gallery height at the site $\vec{i}$ where an intercalant (either A or B) sits. The angular brackets in the second summation are to indicate that each bond $\vec{\delta}$ is only counted once. The terms involving the spring constant K_T and K_F describe, respectively, the transverse and flexural rigidity of the layers.

The host-intercalant interaction is approximated by a harmonic spring of strength $K_{\vec{i}}$ ($=K_A$ or K_B) and equilibrium height $h^0_{\vec{i}}$ ($=h^0_A$ or h^0_B). The energy associated with host layer deformation has two types of contributions common to layered solids. The first one, proportional to K_T, is the transverse layer rigidity, and the second one, proportional to K_F, is the flexural rigidity.[13,14] For binary systems, i.e., AL or BL, all the h's are equal and the gallery height (or equivalently the interlayer spacing) is $h=h^0_A$ or $h=h^0_B$.

In a continuum model, the terms involving K_T and K_F in Eq. (1) give an energy density

$$\frac{1}{2a}[(z\delta^2/2d)K_T(\nabla h)^2+(z\delta^2/2d)^2K_F(\nabla^2 h)^2] , \tag{2}$$

where a is the area per atom, z is the number of nearest neighbors, and d is the dimension ($d=1$ or 2 in this work). This leads to an equation of motion,

$$\rho a\frac{\partial^2}{\partial t^2}h=(z\delta^2/2d)K_T\nabla^2 h-(z\delta^2/2d)^2K_F\nabla^4 h , \tag{3}$$

where $h(x,y,t)$ is the height, $\nabla=(\partial/\partial x,\partial/\partial y)$ is the two-dimensional gradient operator, and ρ is the mass density. From Eq. (3), we see that the isotropic layer dispersion relation at long wavelengths is

$$\omega_q^2=\frac{1}{\rho a}[(z\delta^2/2d)K_Tq^2+(z\delta^2/2d)^2K_Fq^4] , \tag{4}$$

where q is the wave vector.

One can define several average heights for this problem. These are $\langle h\rangle$, $\langle h_A\rangle$, and $\langle h_B\rangle$ where

$$\langle h\rangle=\frac{1}{N}\sum_{\vec{i}}h_{\vec{i}} \tag{5}$$

with similar expression for $\langle h_A\rangle$ and $\langle h_B\rangle$ with the averages restricted to sites occupied by A- or B-type atoms only. To obtain various averaged quantities of interest, one has to minimize the energy E given in Eq. (1) with respect to the heights $h_{\vec{i}}$ for a given realization of the random variables $K_{\vec{i}}$ ($=K_A$ or K_B) and $h^0_{\vec{i}}$ ($=h^0_A$ or h^0_B). We can then calculate $\langle h\rangle$, $\langle h_A\rangle$, $\langle h_B\rangle$, the average energy per site $\varepsilon=E/N$, the fluctuations in height $\langle(h-\langle h\rangle)^2\rangle$, etc., as functions of x, K_A, K_B, h^0_A, h^0_B, K_T, K_F, and the structure of the host lattice by averaging over different configurations.

One simplifying aspect of the harmonic model with uniaxial displacements, which we will refer to as the scalar case, is that we can scale the heights and the energy by $h^0_B-h^0_A$ and $(h^0_B-h^0_A)^2$, respectively. If we define a local dimensionless height $d_{\vec{i}}$ such that

$$h_{\vec{i}}=h^0_A+d_{\vec{i}}(h^0_B-h^0_A) , \tag{6}$$

where $d_{\vec{i}}=0$ or 1, then the energy D can be rewritten as

$$E=\tfrac{1}{2}(h^0_B-h^0_A)^2\left[\sum_{\langle\vec{i},\vec{\delta}\rangle}K_T(d_{\vec{i}}-d_{\vec{i}+\vec{\delta}})^2 +\sum_{\vec{i}}K_F\left[\sum_{\vec{\delta}}(d_{\vec{i}}-d_{\vec{i}+\vec{\delta}})\right]^2 +\sum_{\vec{i}}{}^AK_Ad_{\vec{i}}^2+\sum_{\vec{i}}{}^BK_B(1-d_{\vec{i}})^2\right] . \tag{7}$$

Here the superscripts A and B on the summations means that the sums go over only the A sites or over the B sites. In the harmonic model the actual value of the difference $h^0_A-h^0_B$ is not relevant for the physical properties of the system as it scales out. This is because all the displacements are in the same direction. The diagram accompanying this scaling transformation is shown in Fig. 2. The particles are attached to the lower or upper surface depending on whether they are A or B. These surfaces are rigidly separated by unit distance and the particles are constrained to move only in a direction perpendicular to the planes. In more complex geometries, such as those in $3d$ mixed semiconductors,[15] the arguments leading to Eqs. (6) and (7) are only correct for small values of the

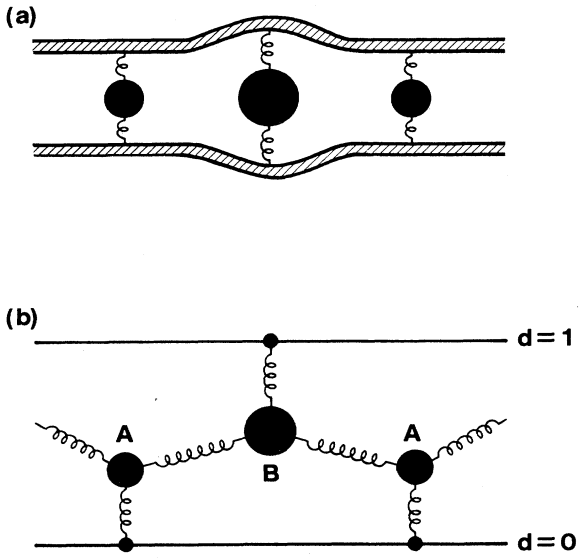

FIG. 2. Side view of the intercalants from Fig. 1, showing a larger B intercalant and two smaller A intercalants. In (a), the separations between the layers are given by the variables h_i, whereas the diagram going with the corresponding dimensionless variables d_i is shown in (b).

natural length differences $h_B^0-h_A^0$. The average height given in Eq. (5) becomes

$$\langle d\rangle=\frac{1}{N}\sum_{\vec{i}} d_{\vec{i}} . \tag{8}$$

Note that by definition

$$\langle d\rangle=(1-x)\langle d_A\rangle+x\langle d_B\rangle . \tag{9}$$

There is no net macroscopic force on the system in equilibrium which leads to the relation

$$(1-x)K_A\langle d_A\rangle=xK_B\langle 1-d_B\rangle . \tag{10}$$

Thus if we know any one of the three quantities $\langle d\rangle$, $\langle d_A\rangle$, and $\langle d_B\rangle$, the other two can be found using Eqs. (9) and (10). The fluctuations in d, d_A, and d_B are related by

$$\begin{aligned}\langle(d-\langle d\rangle)^2\rangle=&(1-x)\langle(d_A-\langle d_A\rangle)^2\rangle\\&+x\langle(d_B-\langle d_B\rangle)^2\rangle\\&+x(1-x)(\langle d_A\rangle-\langle d_B\rangle)^2\end{aligned} \tag{11}$$

which follows directly from the definitions.

III. LIMITING CASES AND EXACT SOLUTIONS

A. Completely floppy and infinitely rigid limits

If the layers are completely floppy towards transverse distortions ($K_T=K_F=0$), then the energy E is minimized trivially. In this limit, we have $\langle d\rangle=x$; the usual Vegard's law[2] with $\langle d_A\rangle=0$ and $\langle d_B\rangle=1$. The corresponding fluctuations are given by $\langle(\Delta d)^2\rangle=\langle d^2\rangle-\langle d\rangle^2=x(1-x)$, and $\langle(\Delta d_A)^2\rangle=\langle(\Delta d_B)^2\rangle=0$ because all the A sites have dimensionless height zero and all the B sites have dimensionless height 1.

In the limit of infinite layer rigidity (i.e., when K_T and/or $K_F\to\infty$), the energy E is minimized by having all the $d_{\vec{i}}$ equal ($d_A=d_B=d$). Here the energy per site,

$$\varepsilon=\tfrac{1}{2}(1-x)K_Ad^2+\tfrac{1}{2}xK_B(1-d)^2 , \tag{12}$$

is minimized by

$$\langle d\rangle=\langle d_A\rangle=\langle d_B\rangle=\frac{xK_B}{xK_B+(1-x)K_A} \tag{13}$$

giving an energy

$$\varepsilon=\tfrac{1}{2}x(1-x)K_AK_B/[xK_B+(1-x)K_A] \tag{14}$$

and fluctuations in all the three heights vanish in this limit. In earlier theoretical studies dealing with the gallery expansion using discreate lattice models, all the $d_{\vec{i}}$'s were assumed to be the same (rigid-layer model[4,9]) even for systems with finite layer rigidity. In this approximation, the non-Vegard's law behavior was determined completely by the compressibility ratio K_A/K_B of the two intercalants. At small x, Eq. (13) becomes $\langle d\rangle\to(K_B/K_A)x$. If the larger ion B is highly incompressible compared to A, i.e., $K_B\gg K_A$, one finds a large deviation (superlinear) from Vegard's law behavior which continues for all x. On the other hand, if the larger ion is more compressible than the smaller ion, then $\langle d\rangle$ shows a deviation from Vegard's law but with sublinear behavior. If $K_B=K_A$, then one observes a Vegard's law behavior even for an infinitely rigid layer. Later, we will show that within our model, Vegard's law is obtained for arbitrary layer rigidity as long as $K_A=K_B$.

B. One-dimensional chain with $K_A=K_B$

To calculate the average quantities exactly for the one-dimensional (1D) chain, it is slightly more convenient to work with the h variables, rather than the dimensionless d variables. One reason for studying the 1D chain problem is that the effective-medium theory which we have developed for this problem (to be discussed in Sec. IV) can be worked out analytically for the 1D case and compared with the exact calculations to test its accuracy. The energy for the 1D chain is given by

$$\begin{aligned}E_{1D}=&\tfrac{1}{2}\sum_i K_i(h_i-h_i^0)^2+\tfrac{1}{2}K_T\sum_i(h_i-h_{i+1})^2\\&+\tfrac{1}{2}K_F\sum_i(2h_i-h_{i+1}-h_{i-1})^2 .\end{aligned} \tag{15}$$

Minimizing E_{1D} with respect to the h_i, we find

$$\mathbf{M}\mathbf{h}=\boldsymbol{\phi} , \tag{16}$$

where $\mathbf{M}$ is a tridiagonal matrix with random diagonal

matrix elements, i.e.,

$$M_{ii}=K_i+2K_T+6K_F\ ,$$
$$M_{i,\,i\pm1}=-K_T-4K_F\ , \tag{17}$$
$$M_{i,\,i\pm2}=K_F\ ,$$
$$\mathbf{h}=(h_1,h_2,\ldots,h_N),\quad \boldsymbol{\phi}^{\dagger}=(K_1h_1^0,K_2h_2^0,\ldots,K_Nh_N^0)\ . \tag{18}$$

In Eqs. (15)–(18), all quantities are real. When both K_i and h_i^0 are random variables, which is the case when $K_A\neq K_B$, the problem is difficult to solve analytically. Our numerical solutions in this case will be discussed in Sec. IV. However, when $K_A=K_B=K$, one can obtain the h_i's by diagonalizing the **M** matrix, which is no longer random. In this case, the results can be worked out analytically. In this limit, the eigenvalues λ_q and eigenvectors $\psi_q(i)$ of the matrix **M** are given as

$$\lambda_q=K+2K_T[1-\cos(q,\delta)]+4K_F[1-\cos(q\delta)]^2 \tag{19}$$

and

$$\psi_q(n)=\frac{1}{\sqrt{N}}\exp(iqn) \tag{20}$$

with $q=2\pi r/N$ with $r=0,1,2,\ldots,N-1$. Then we have

$$\langle h\rangle=\frac{1}{N}\sum_{ij}(\mathbf{M}^{-1})_{ij}\phi_j=\frac{1}{N}\sum_q\sum_{i,j}\frac{K}{\lambda_q}\psi_q(i)\psi_q^*(j)h_j^0$$
$$=\frac{K}{\lambda_0 N}\sum_i h_i^0=xh_B^0+(1-x)h_A^0\ . \tag{21}$$

Thus we recover $\langle d\rangle=x$, i.e., Vegard's law behavior, for all values of K_T. However, the site-specific-gallery heights $\langle d_A\rangle$ and $\langle d_B\rangle$ do depend on the layer-rigidity parameters K_T, K_F through the relation

$$\langle d_A\rangle=x[1-W(K)]$$

and

$$\langle d_B\rangle=1-(1-x)[1-W(K)]\ . \tag{22}$$

The Watson integral $W(K)$ is discussed and calculated in Appendix A. Note that the expressions in Eq. (22) obey the general relation in Eq. (10). As the general expression for $W(K)$ given in Appendix A is rather complex, we give the results here for $K_F=0$. We find

$$\langle d_A\rangle=x[1-(1+4K_T/K)^{-1/2}] \tag{23}$$

and

$$\langle d_B\rangle=1-(1-x)[1-(1+4K_T/K)^{-1/2}]\ . \tag{24}$$

Clearly when $K_T=K_F=0$, i.e., in the floppy layer limit, these results [Eqs. (23) and (24)] become $\langle d_A\rangle=0$ and $\langle d_B\rangle=1$ and when K_T or $K_F=\infty$, i.e., the infinitely rigid-layer limit, $\langle d_A\rangle=\langle d_B\rangle=x$. Thus, in the limit $K_A=K_B$, when $\langle d\rangle$ shows a Vegard's law behavior the transverse layer-rigidity effects are seen in the x dependence of $\langle d_A\rangle$ and $\langle d_B\rangle$. This point will be discussed in more detail later.

The energy and the fluctuations in d, d_A, and d_B can also be calculated in this limit. We obtain

$$\varepsilon=\tfrac{1}{2}Kx(1-x)[1-W(K)]=\tfrac{1}{2}Kx(1-x)[1-(1+4K_T/K)^{-1/2}]\ , \tag{25}$$
$$\langle(d_A-\langle d_A\rangle)^2\rangle=\langle(d_B-\langle d_B\rangle)^2\rangle=x(1-x)[W_1(K)-W(K)^2]$$
$$=x(1-x)[(1+2K_T/K)(1+4K_T/K)^{-1/2}-1]/(1+4K_T/K)\ , \tag{26}$$
$$\langle(d-\langle d\rangle)^2\rangle=x(1-x)W_1(K)=x(1-x)(1+2K_T/K)(1+4K_T/K)^{-3/2}\ , \tag{27}$$

where the explicit results in Eqs. (25)–(27) have $K_F=0$ for simplicity. From the above equations we see that the fluctuations are maximum when $x=0.5$ and $K_T=0$ as would be expected. Note that the expressions for the fluctuations in Eqs. (26) and (27) obey the general result Eq. (11). The results for a linear chain with $K_A=K_B=K=K_T$ and $K_F=0$ are shown in Fig. 3 together with simulation results obtained by the method described in Sec. V.

C. Two-dimensional lattice with $K_A=K_B$

The average energy, average gallery heights, and the corresponding fluctuations can also be calculated exactly for 2D systems in the limit $K_A=K_B=K$. One has to replace $\lambda_{\vec{q}}$ in the Watson integrals used in Sec. III B by

$$\lambda_{\vec{q}}=K+K_Tz(1-\gamma_{\vec{q}})+K_F[z(1-\gamma_{\vec{q}})]^2\ , \tag{28}$$

where

$$\gamma_{\vec{q}}=\frac{1}{z}\sum_{\vec{\delta}}e^{i\vec{q}\cdot\vec{\delta}} \tag{29}$$

and z is the number of nearest neighbors ($z=4$ for the square lattice, $z=6$ for the triangular net). Clearly the geometry of the lattice will determine $\lambda_{\vec{q}}$ and hence the layer distortion characteristics. The results are formally the same as for the linear chain, except that the appropriate Watson integrals from Appendix A for two dimensions must be used in Eqs. (22) and (25)–(27). The average height obeys Vegard's law in this limit for all lattices. We will compare these exact results with numerical simulations in Sec. V.

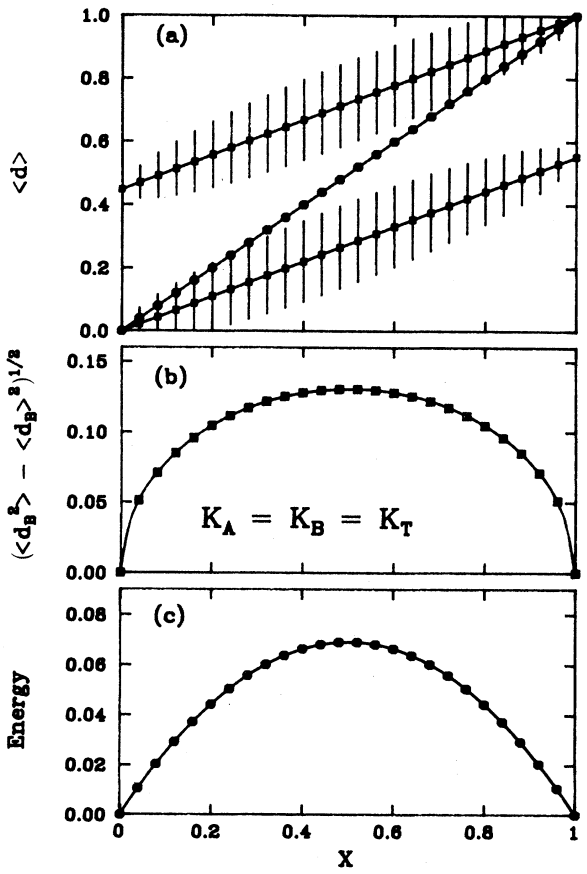

FIG. 3. Showing (a) average height, (b) fluctuations in height, and (c) the energy in units of $\frac{1}{2}K(h_B^0-h_A^0)^2$, for a one-dimensional chain with $K_A=K_B$. The solid lines are exact results and the solid dots represents simulation results.

IV. EFFECTIVE-MEDIUM THEORY

In this section we develop an effective-medium theory. The work in this section follows the general ideas of Feng, Thorpe, and Garboczi.[16] The effect of the layers on the intercalant atom is contained within an effective layer spring constant K_e. This can be found by applying a force F to a single site 0 in the nonrandom system where $K=K_A=K_B$ as shown in Fig. 4(a). The equation of motion is

$$F=-\frac{\partial E}{\partial h_0} \tag{30}$$

where the energy E is given in Eq. (1). The right-hand side of this equations is linear in the $\{h_i\}$ and can be inverted to give the diagonal term

$$h_0=W(K)F\ , \tag{31}$$

where the effective spring constant for this kind of displacement K_e is given by

$$K_e=K/W(K) \tag{32}$$

and $W(K)$ is the same Watson integral that we used in the preceding section. The whole system is replaced by a single spring K_e as shown in Fig. 4(b). The problem is now reduced to just two springs as shown in Fig. 5. One of these springs is K_α, where α can be either A or B with probability $1-x$ or x, respectively. The other spring is $K_e'=K_e-K$, formed by removing the spring K which is in parallel. The total energy per site ε for a single impurity is given by

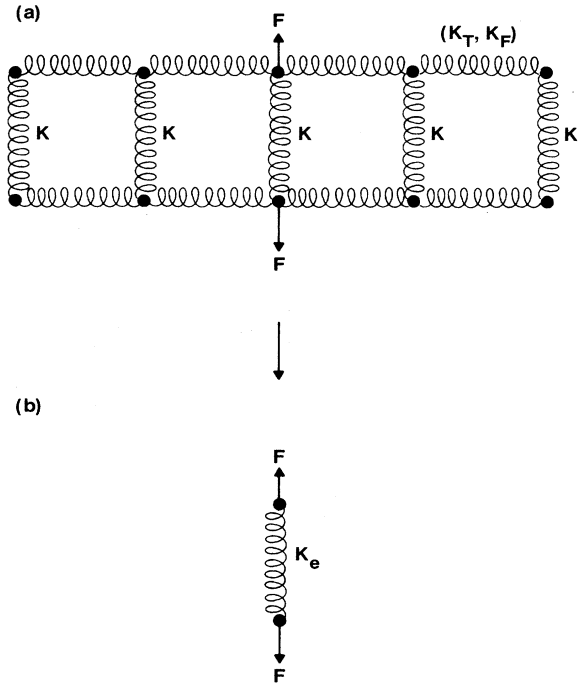

FIG. 4. Illustrating how the equivalent spring K_e is determined within effective-medium theory.

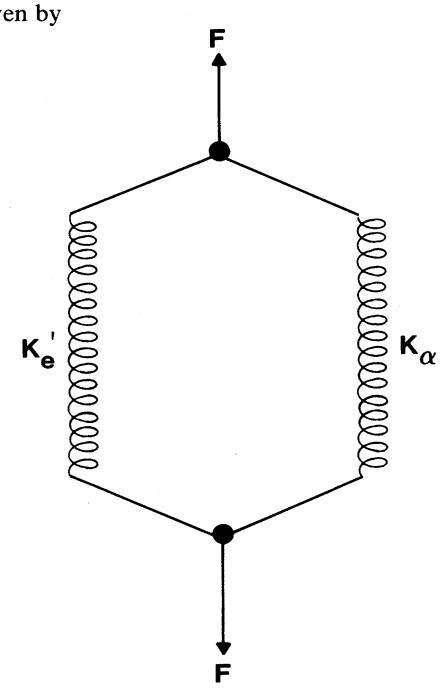

FIG. 5. Showing how the local rigidity is determined within effective- medium theory. Here $K_e'=K_e-K$ and $\alpha=A$ or B.

$$\varepsilon=\tfrac{1}{2}K_e'(h-h_e)^2+\tfrac{1}{2}K_\alpha(h-h_\alpha^0)^2 \tag{33}$$

where h_e is the effective height which like the effective spring constant K_e is to be determined self-consistently. We are considering only a single impurity spring K_α in Eq. (33). We minimize the energy ε with respect to h and obtain the local height h,

$$h=(K_e'h_e+K_\alpha h_\alpha^0)/(K_e'+K_\alpha)\ . \tag{34}$$

Substituting this back in Eq. (33) gives the energy for a single impurity

$$\varepsilon=\tfrac{1}{2}(h_e-h_\alpha^0)^2K_e'K_\alpha/(K_e'+K_\alpha)\ . \tag{35}$$

Because the springs have different lengths, the post factor in Eq. (35) comes from adding the two springs in series. A general energy expression can be written down by summing over all the different types of impurities which in the spirit of effective-medium theory are assumed to be noninteracting:

$$\varepsilon=\tfrac{1}{2}\sum_\alpha p_\alpha(h_e-h_\alpha^0)^2K_e'K_\alpha/(K_e'+K_\alpha)\ . \tag{36}$$

This expression contains two unknown parameters, the height h_e and the spring constant K_e' (or equivalently K_e or K). These are determined by two conditions. For the first we minimize the energy ε with respect to h_e to give

$$h_e=\frac{\sum_\alpha p_\alpha h_\alpha^0K_\alpha/(K_e'+K_\alpha)}{\sum_\alpha p_\alpha K_\alpha/(K_e'+K_\alpha)}\ . \tag{37}$$

This expression can be regarded as variational because a minimization is involved. Unfortunately we have not been able to derive a second condition variationally. Instead we use the following argument. Apply a force $\vec{F}$ at the single impurity site. This produces a displacement $\vec{F}/(K_e'+K_\alpha)$ which when averaged over all sites is set equal to $\vec{F}/K_e$ to give the self-consistency condition

$$\sum_\alpha p_\alpha/(K_e'+K_\alpha)=1/K_e \tag{38}$$

which for the case of interest here with two intercalants A,B can be written as

$$x(K-K_B)/(K_e'+K_B)+(1-x)(K-K_A)/(K_e'+K_A)=0\ . \tag{39}$$

Various solutions for K from Eq. (39) are shown in Fig. 6 for the triangular net and compared to the virtual-crystal result $K=xK_B+(1-x)K_A$. It can be seen that the results used here, which agree very well in simulations as discussed in the next section, are very different from the virtual-crystal result. Together Eqs. (37) and (38) provide the effective-medium solution to the problem. Combining the two, we can rewrite Eq. (37) as

$$h_e=\sum_\alpha p_\alpha h_\alpha^0KK_\alpha/[K_e(K_e'+K_\alpha)] \tag{40}$$

which for the case of the two intercalants A,B of interest here, can be written in terms of the dimensionless heights d as

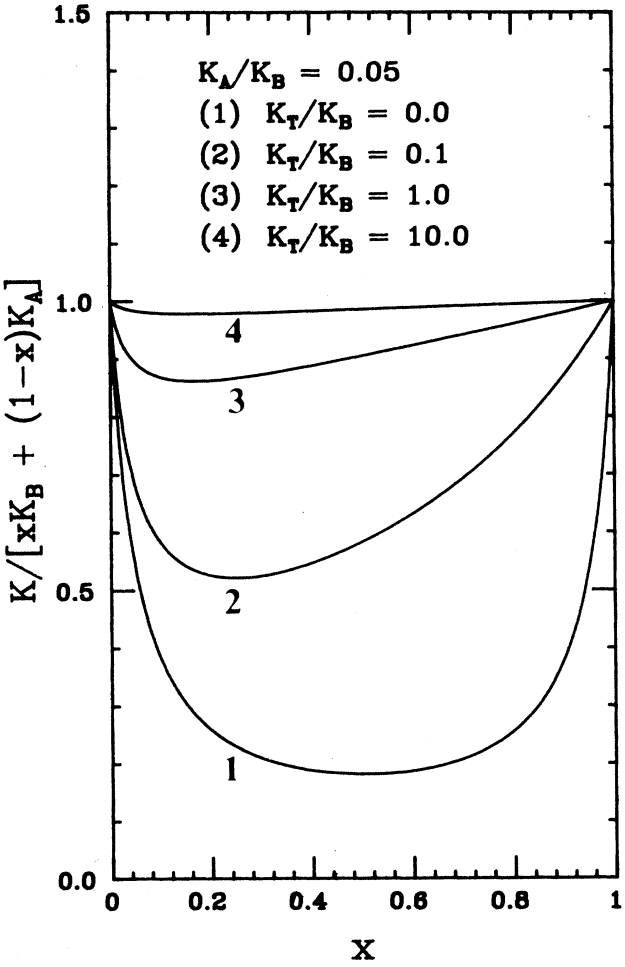

FIG. 6. The spring constant K of the effective medium for a triangular lattice is compared to the virtual-crystal result $xK_B+(1-x)K_A$.

$$\langle d\rangle=(h-h_A^0)/(h_B^0-h_A^0)$$
$$=\frac{xK_B/(K_e'+K_B)}{xK_B/(K_e'+K_B)+(1-x)K_A/(K_e'+K_A)} \tag{41}$$

which after some manipulation can be put into the form

$$\langle d\rangle=x+x(1-x)F_d$$

where

$$F_d=[K_eK_e'(K_B-K_A)]/[K(K_e'+K_A)(K_e'+K_B)]\ . \tag{42}$$

Either directly, or using Eqs. (9) and (10), we can find $\langle d_A\rangle$ and $\langle d_B\rangle$:

$$\langle d_A\rangle=xK_eK_e'K_B/[K(K_e'+K_A)(K_e'+K_B)]\ ,$$
$$\langle d_B\rangle=1-(1-x)K_eK_e'K_A/[K(K_e'+K_A)(K_e'+K_B)]\ . \tag{43}$$

The energy can also be found by substituting Eqs. (39)

and (40) back into Eq. (36), and using the probabilities appropriate to two kinds of sites. We find

$$\varepsilon=\tfrac{1}{2}(K_A K_B)^{1/2}x(1-x)(h_B^0-h_A^0)^2F_\varepsilon\ , \tag{44}$$

where

$$F_\varepsilon=[K_e K_e'(K_A K_B)^{1/2}]/[K(K_e'+K_A)(K_e'+K_B)]\ . \tag{45}$$

The effective spring constants K, $K_e=K_e'+K$ are determined by Eq. (39). We note that

$$F_d/F_\varepsilon=(K_B-K_A)/(K_A K_B)^{1/2} \tag{46}$$

gives a useful relation as it is independent of any of the effective-medium parameters. Although the derivation of Eq. (46) is within effective-medium theory, it is in fact an exact relation as can be proved using the Feynman-Hellman theorem.[17] In the present context, this theorem states that

$$\frac{\partial}{\partial p}\langle\varepsilon\rangle=\left\langle\frac{\partial\varepsilon}{\partial p}\right\rangle \tag{47}$$

where the energy $\varepsilon=E/N$ depends on some parameter p. From Eq. (1), we see that p can be set equal to h_A^0 or h_B^0, which leads to Eqs. (9) and (10) and also allows us to demonstrate that Eq. (46) is an exact result. Of course effective-medium results are exact in the limit of single impurities where the linear terms in x or $1-x$ are given correctly in all quantities that we have calculated. Explicit results in this limit can be found from Eqs. (41)–(46) and for small x are

$$\langle d\rangle=x(K_B/K_A)/[1+(K_B/K_A-1)W(K_A)]\ ,$$

$$\langle d_A\rangle=x(K_B/K_A)\times[1-W(K_A)]/[1+(K_B/K_A-1)W(K_A)]\ ,$$

$$\langle d_B\rangle=(K_B/K_A)W(K_A)/[1+(K_B/K_A-1)W(K_A)]\ ,$$

$$\varepsilon=\tfrac{1}{2}K_B x(h_B^0-h_A^0)^2\times[1-W(K_A)]/[1+(K_B/K_A-1)W(K_A)]\ . \tag{48}$$

Similar expressions for small $1-x$ can be found by replacing x by $1-x$, d by $1-d$, and interchanging A and B in Eqs. (48).

The effective-medium results derived in this section contain the previous, exact results as special cases. For infinitely rigid layers, when K_T or K_F are infinite as discussed in Sec. III A, Eq. (39) becomes $K=xK_B+(1-x)K_A$ and the effective-medium results of this section reduce to Eqs. (13) and (14). When $K_A=K_B=K$, using Eq. (32) that relates K_e to the Watson integral $W(K)$, we recover the results of Sec. III B and III C for $\langle d\rangle$, $\langle d_A\rangle$, $\langle d_B\rangle$, and ε.

The fluctuations cannot be easily calculated within effective-medium theory. However, they can be obtained, through the back door, using the Feynman-Hellman theorem Eq. (47), with p set equal to K_A and K_B, respectively. Using the effective medium Eq. (39) and differentiating (24) with respect to K_A, we find after considerable algebra

$$\langle(d_A-\langle d_A\rangle)^2\rangle=\frac{x(1-x)\left[\dfrac{K_A K_B K_e^2}{K(K_e'+K_A)^2(K_e'+K_B)}\right]^2}{\dfrac{[W(K)]^2}{W_1(K)-[W(K)]^2}+\dfrac{(K-K_A)(K-K_B)}{(K_e'+K_A)(K_e'+K_B)}}\ , \tag{49}$$

and a similar expression for $\langle(d_B-\langle d_B\rangle)^2\rangle$ with A and B interchanged in Eq. (49). Using Eq. (49), the fluctuations in d can be found using Eq. (11). We write

$$\langle(d-\langle d\rangle)^2\rangle=\frac{x(1-x)\left[\dfrac{K_A K_B K_e}{K(K_e'+K_A)(K_e'+K_B)}\right]^2\dfrac{W_1(K)}{W_1(K)-[W(K)]^2}}{\dfrac{[W(K)]^2}{W_1(K)-[W(K)]^2}+\dfrac{(K-K_A)(K-K_B)}{(K_e'+K_A)(K_e'+K_B)}}\ . \tag{50}$$

We note that in the limit $K_A=K_B=K$, the exact results Eqs. (26) and (27) are recovered. Thus the use of the Feynman-Hellman theorem allows us to extract the fluctuations in d. Without the use of this theorem it would not be possible to obtain these fluctuations in an effective-medium theory. In the next section, we test how good the effective-medium approximation is in general, by comparing results with numerical simulations. We stress that in the appropriate limits, the effective-medium results derived in this section reproduce all the exact results of Sec. II. In particular, the completely floppy ($K_T=K_F=0$), the infinitely rigid ($K_T=K_F\to\infty$), and the $K_A=K_B$ cases are all given correctly.

V. NUMERICAL SIMULATIONS

In this section we describe our numerical simulation procedures and analyze the results obtained. We will also compare these numerical results with the same quantities from our exact solutions when $K_A=K_B$ and from the effective-medium theory when $K_A\neq K_B$. The problem of finding the stable structure of the random alloy can by regarded as an optimization problem for the energy function Eq. (1). To find the equilibrium structure, the total energy is minimized with respect to the variables $\{h_i\}$. At zero temperature, the minimization procedure we have used is based on the conjugate gradient method.[18,19]

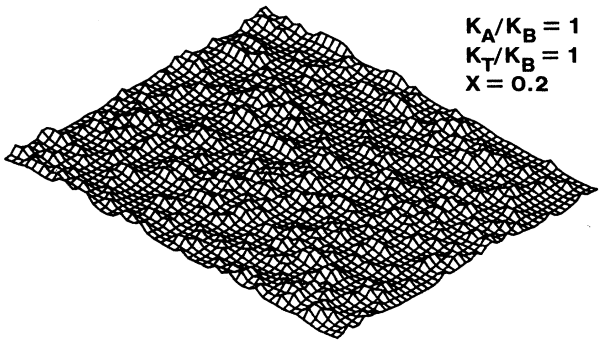

FIG. 7. A configuration of a relaxed triangular layer with $K_A/K_B=1.0$, $K_T/K_B=1.0$ and $x=0.2$. This result is obtained from simulation.

We have found that this method is more powerful in terms of computer time and accuracy compared with other methods such as direct matrix diagonalization or the relaxation method.[16] We have performed extensive studies for the triangular lattice were typical lattice sizes used were $N=50\times50=2500$ nodes with periodic boundary conditions. We have chosen the values of our parameters to be close to those of Li and vacancies in graphite,[5,6] and K and Rb in graphite.[7,8] The details of the numerical procedure consist of the following steps for each concentration x.

(a) First an initial configuration is generated. This was done by generating a two-dimensional triangular network of N nodes with each node labeled sequentially and assigning vertical springs K_A and local heights h_A^0 at each node. Then we randomly select an A-type node and replace it by a vertical spring K_B and local height h_B^0 until the total number of B-type nodes is $N_B=xN$. All nearest-neighbor horizontal springs are uniform and given by K_T (and K_F).

(b) The system is relaxed using the conjugate gradient total energy minimization method.[18,19] A final configuration characterized by heights $\{h_i\}$ is obtained.

(c) The average height, fluctuations in height and average energy, etc., are obtained at the equilibrium configuration.

(d) The above steps are repeated 1000 times to obtain an ensemble average.

These numerical simulation procedures were carried out for several values of K_A, K_B, and K_T (while keeping $K_F=0$). Figure 7 shows a typical configuration of the relaxed layer at $x=0.2$. One sees the relaxed layer is not flat, but rather has the appearance of "waves on the ocean." As $K_T\to\infty$, the layers do become flat as dis-

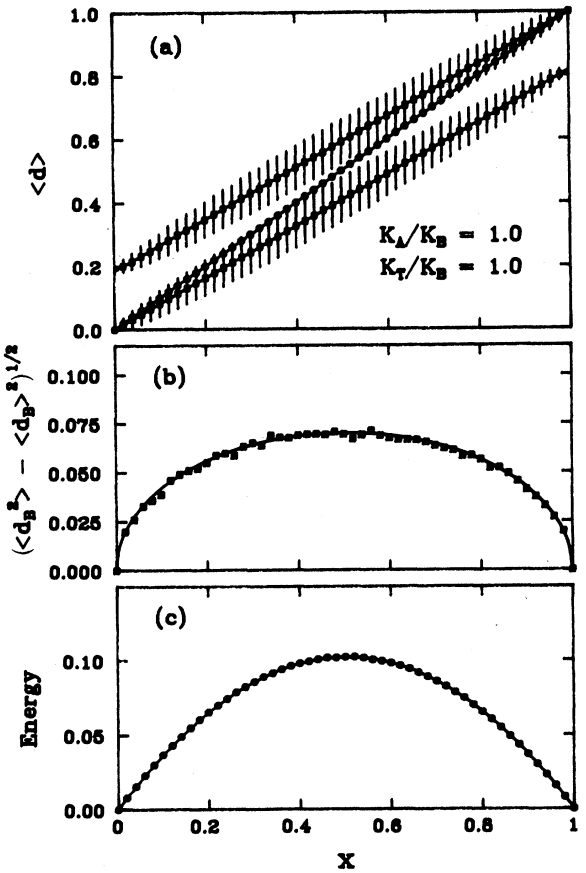

FIG. 8. Showing (a) average height, (b) fluctuations in height, and (c) the energy in units of $\frac{1}{2}K(h_B^0-h_A^0)^2$, for a triangular net with $K_A=K_B=K_T$. The solid lines are exact results and the solid dots represent simulation results.

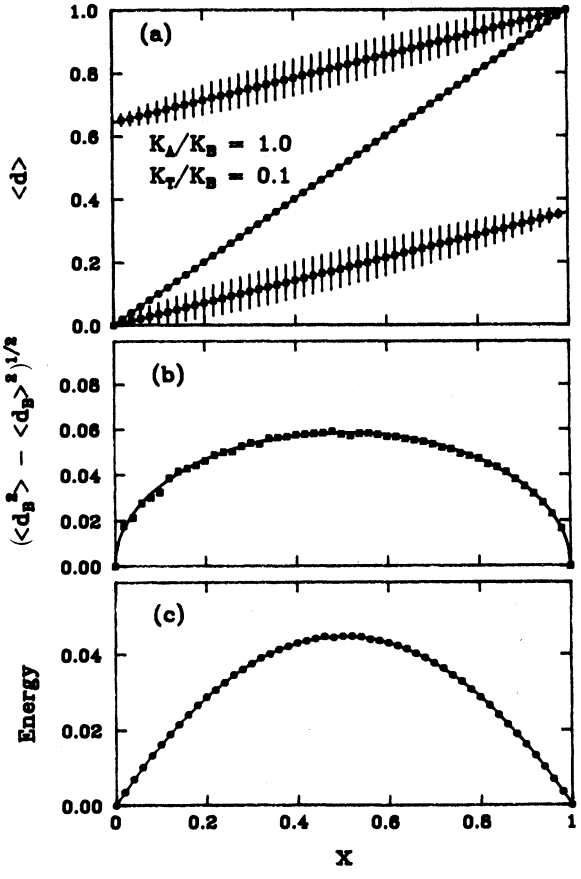

FIG. 9. Showing (a) average height, (b) fluctuations in height, and (c) the energy in units of $\frac{1}{2}K(h_B^0-h_A^0)^2$, for a triangular net with $K_A=K_B\neq K_T$. The solid lines are exact results and the solid dots represent simulation results.

cussed in Sec. III A.[4] The simulation results of the average heights, average fluctuations for both the A and B intercalants, and the energy are shown as solid dots in Figs. 8–11. These figures are all for the triangular lattice. In Figs. 8 and 9, the simulation results are compared to the exact solution. The agreement is excellent for all quantities, thereby giving us confidence in our simulations in that we are using large enough lattices, etc. In Figs. 10 and 11, the solid lines are the effective-medium results for the above quantities. The effective-medium results provide excellent fits to the simulation results. Indeed the quality of the fits is almost as good as for the exact results in Figs. 8 and 9, except perhaps for the fluctuations in d_α (with $\alpha = A,B$) where there appear to be small systematic differences. The effective-medium results are exact for small x and small $1-x$. However, effective-medium theory is only an approximation in general as shown in Appendix B. Nevertheless the quality of the agreement in Figs. 10 and 11 is excellent and means that effective-medium theory can be used with considerable confidence in interpreting experimental data.

When $K_A = K_B$, the average heights $\langle d \rangle$, $\langle d_A \rangle$, $\langle d_B \rangle$ show straight line behavior; with $\langle d \rangle$ obeying Vegard's law. The fluctuations and average energy are symmetric about $x = 0.5$. The difference

$$\langle d_B \rangle - \langle d_A \rangle = W(K) \tag{51}$$

is independent of x, as can be seen from Eqs. (22) and is illustrated in Figs. 8 and 9. This difference depends strongly on the transverse layer-rigidity parameter K_T and decreases as the rigidity of the layer increases. In the limit of a single B impurity in an A host, we have $\langle d_B \rangle = W(K)$ from Eq. (22). Thus for rather stiff layers, as in Fig. 8, this intercept is quite small ~ 0.2, whereas for rather floppy layers, as in Fig. 9, the intercept increases to ~ 0.65. For infinitely rigid layers $W(K)=0$ and for perfectly floppy layers $W(K)=1$. Thus we can say that $W(K)$ is, through (51), a direct measure of the "floppiness" of the lattice with $0 < W < 1$. Conversely $1-W$ may be regarded as a measure of the rigidity of the lattice. Note that the strain energy ε in the lattice, given in Eq. (25), is also directly proportional to the rigidity of the lattice. For a completely floppy lattice, the strain energy is zero as the lattice can accommodate any impurity at no cost in energy.

When $K_B > K_A$ (Figs. 10 and 11), the average height shows superlinear behavior and the partial heights associated with A and B intercalants are no longer linear. The average energies and fluctuations are peaked at $x < 0.5$,

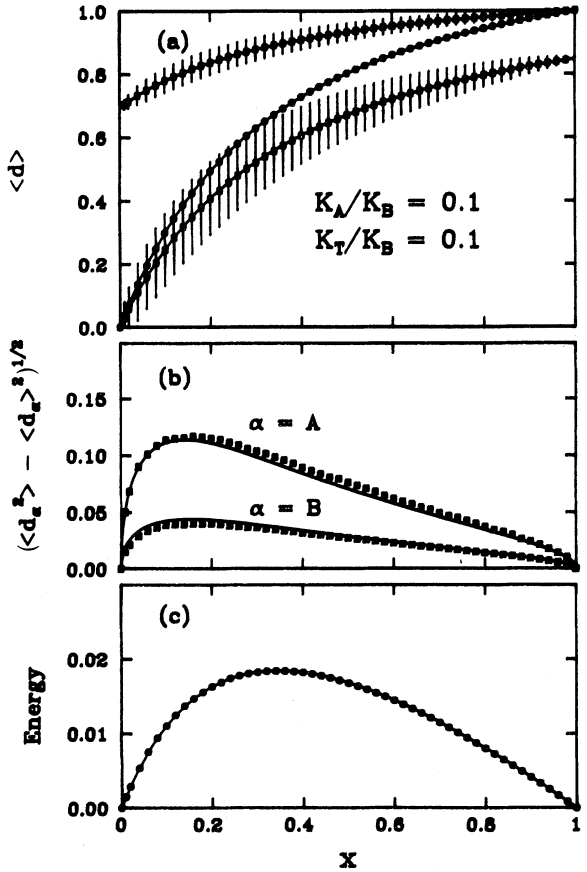

FIG. 10. Showing (a) average height, (b) fluctuations in height, and (c) the energy in units of $\frac{1}{2}(K_A K_B)^{1/2}(h_B^0 - h_A^0)^2$, for a triangular net with $K_A \neq K_B$. The solid lines show results from effective-medium theory and the solid dots represent simulation results.

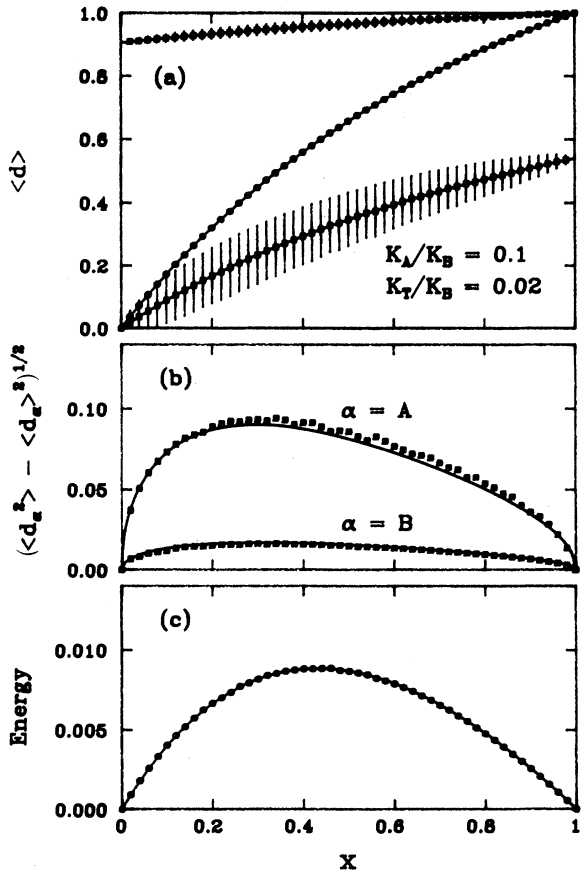

FIG. 11. Showing (a) average height, (b) fluctuations in height, and (c) the energy in units of $\frac{1}{2}(K_A K_B)^{1/2}(h_B^0 - h_A^0)^2$, for a triangular net with $K_A \neq K_B$. The solid lines show results from effective-medium theory and the solid dots represent simulation results.

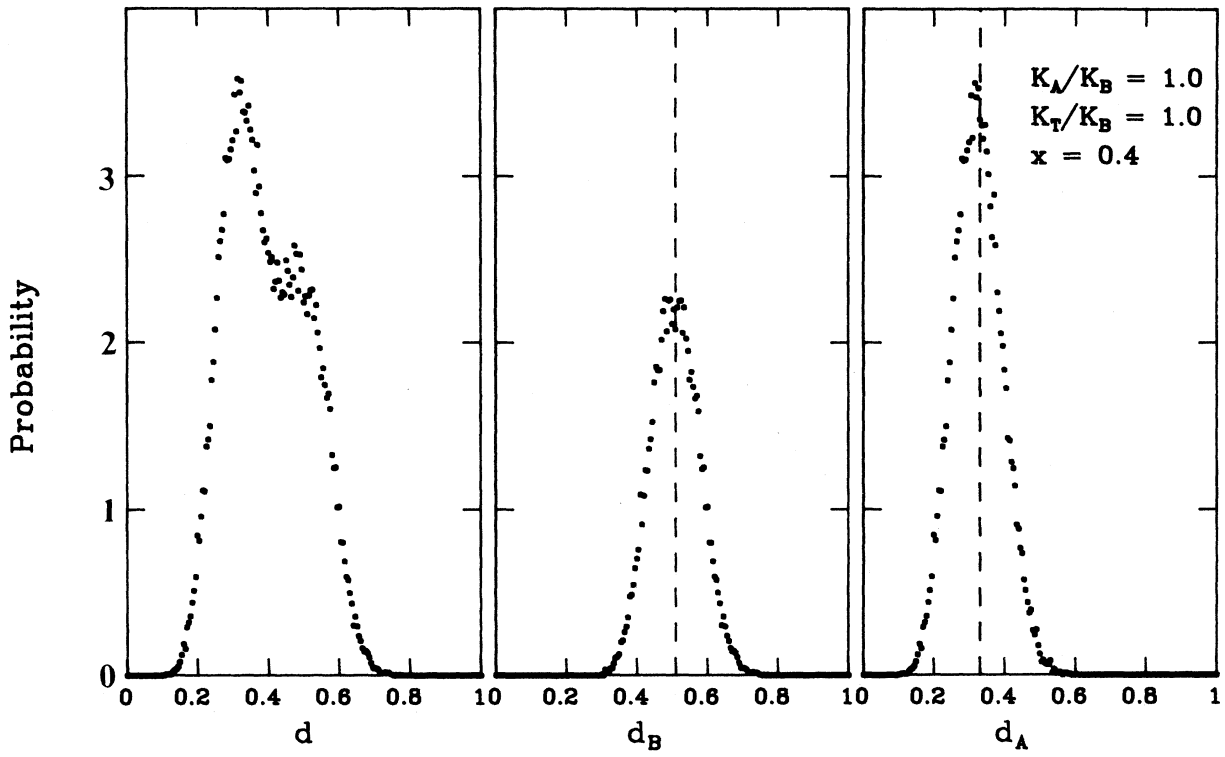

FIG. 12. Probability distributions of d, d_A, and d_B for a 50×50 triangular lattice with $K_A=K_B$. These results are from computer simulations and averaged over 1000 configurations. The vertical dashed lines show $\langle d_A \rangle$ and $\langle d_B \rangle$.

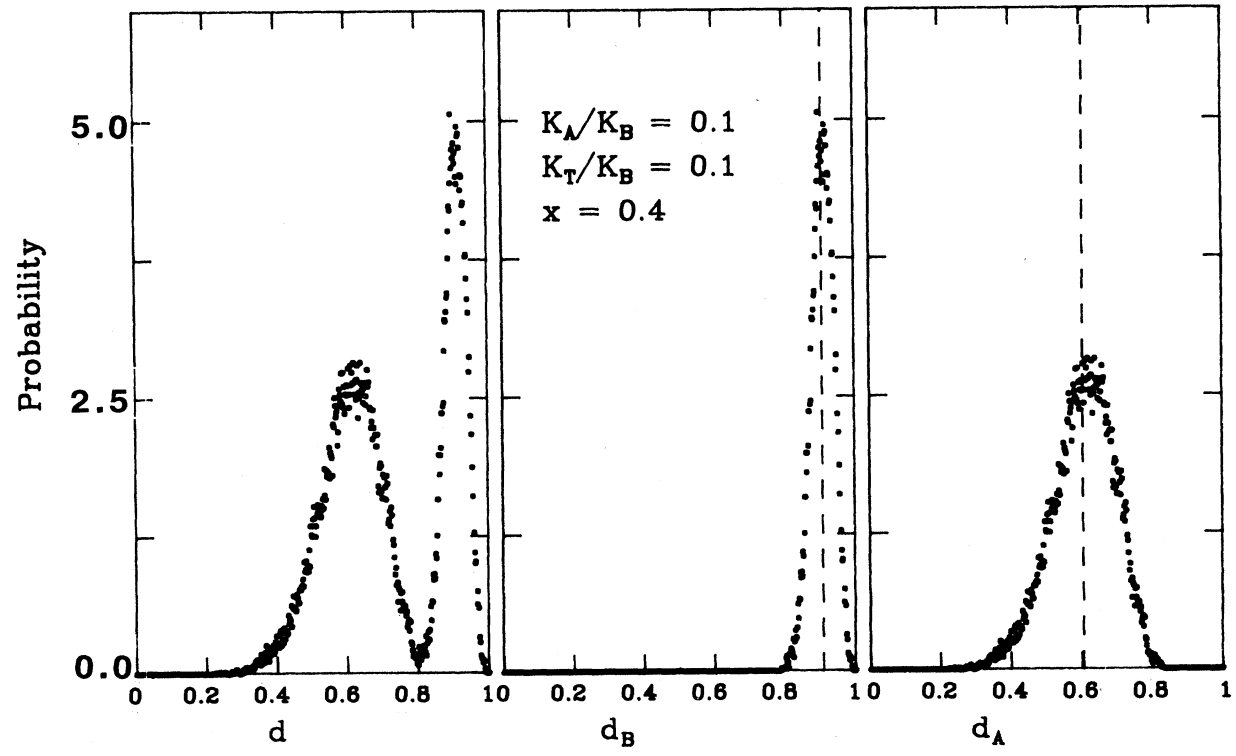

FIG. 13. Probability distributions of d, d_A, and d_B for a 50×50 triangular lattice with $K_A\neq K_B$. These results are from computer simulations and averaged over 1000 configurations. The vertical dashed lines shown $\langle d_A \rangle$ and $\langle d_B \rangle$.

and no longer symmetric about $x=0.5$. Effective-medium theory reproduces the simulation results quite accurately when $K_A \neq K_B$.

The nature of the disorder effect in the structure of random alloy can be better determined by the partial probability distribution functions of the heights for the A- and B-type intercalants. The height probability distributions $P(d)$, $P(d_B)$, $P(d_A)$ are defined by

$$P(d)=\frac{1}{N}\sum_{i=1}^{N}\delta(d-d_i) \tag{52}$$

and

$$P(d_\alpha)=\frac{1}{N_\alpha}\sum_{i=1}^{N_\alpha}\delta(d-d_i), \quad \alpha=A,B \ . \tag{53}$$

We plot these distribution functions obtained from the simulation in Figs. 12 and 13. Figures 12 shows the probability distribution at $x=0.4$ for a system with $K_A=K_B=K_T$. One sees that $P(d_A)$ and $P(d_B)$ are symmetric around the average values $\langle d_A \rangle$ and $\langle d_B \rangle$. The line shapes of the two peaks are close to Gaussian, since from the simulation results, the moment ratio $\langle(\Delta d_\alpha)^4\rangle/\langle(\Delta d_\alpha)^2\rangle^2=2.8\pm0.1$, which is close to the 3 which would be obtained for a Gaussian. The result cannot be exactly a Gaussian, as the distributions are bounded, whereas the Gaussian distribution is unbounded. When $K_A=K_B$, it is possible to calculate the low moments exactly as shown in Sec. III B, but we have not been able to obtain the complete distribution function analytically. Figure 13 shows the probability distributions at $x=0.4$ for a system with $K_T=K_A=0.1K_B$. It is very clear that $P(d_B)$ and especially $P(d_A)$ are not symmetric in this case.

VI. SUMMARY

We have set up a spring model that describes the properties of randomly intercalated layer materials. This model incorporates both the layer rigidity and the compressibilities of the intercalants. We have performed computer simulations for a triangular net geometry. When $K_A=K_B$, the model is exactly soluble, and when $K_A \neq K_B$, we have shown that effective-medium theory gives very good agreement with the simulations. Vegard's law is only obtained, within these models, when $K_A=K_B$; a situation that rarely occurs in practice. When $K_A=K_B$, the effective-medium solution reproduces the exact solution.

These 2D alloy systems provide an almost ideal arena for studying competition between the lattice rigidity and the natural local bond lengths favored by the A and B atoms. To date there is very little data in layered compounds beyond the mean c-axis dimension $\langle h \rangle$ as determined by x-ray Scattering.[6] The two ternary graphite intercalation systems whose average c-axis separation can be understood within our model are $V_{1-x}Li_xC_6$ (Ref. 5) (V is a vacancy) and $K_{1-x}Rb_xC_8$.[7] For the lithium ternary, where the gallery expands from 3.36 Å for $x=0$ to 3.78 Å for $x=1$, the A atom is actually a vacancy so that $K_B/K_A \gg 1$. We have not attempted to fit the experimental data precisely but a choice of $K_A/K_B=0.1$, and $K_T/K_B=0.1$ [see Fig. 10(a)] can semiquantitatively fit the experimental data excepting for $x \approx 1$ where anharmonicity effects may be important. The potassium-rubidium ternary data, where the gallery expands from 5.47 Å for $x=0$ to 5.68 Å for $x=1$, shows nearly a Vegard's law behavior.[7] This can be understood if we assume that $K_A/K_B \approx 1$ which seems physically reasonable. In this case the strength of the layer rigidity can only be determined from measurements of local quantities such as $\langle d_A \rangle$ and $\langle d_B \rangle$. We would very much like to see experiments performed that couple to these local structural parameters. This could be done using extend x-ray-absorption fine structure[20] (EXAFS) or NMR.[21] The experimental situation is more advanced for mixed semiconducting alloys[22] such as $Ga_xIn_{1-x}As$, where many compounds have been studied using both x-rays and EXAFS. The results[22] for $\langle d \rangle$, $\langle d_A \rangle$, and $\langle d_B \rangle$ are remarkably similar to those we have obtained in Fig. 9. This will be further discussed in a subsequent publication.[23]

The results obtained in this paper are more general than the simple geometries and force constant models that we have used. These have served our purpose in il-

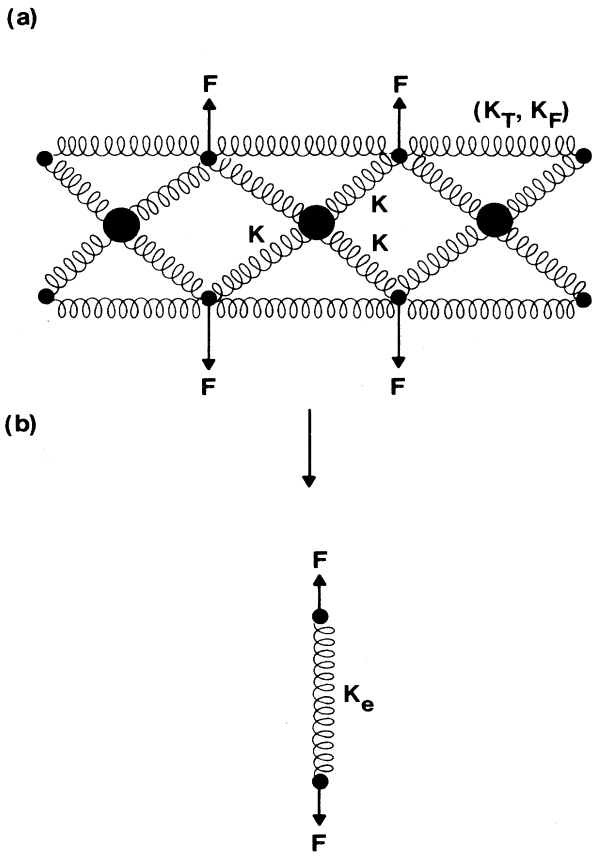

FIG. 14. An illustration of the side view of a more complex lattice than shown in Fig. 4. The equivalent spring K_e can be determined within effective-medium theory if appropriate forces F are applied as shown.

lustrating the kinds of behavior to be expected. However, effective force constants can be defined for more complex geometries as illustrated in Fig. 14. Here the intercalant atoms have many springs attached to common points in the layers above and below. By applying a suitable force field, as illustrated, an effective force constant K_e can be defined that leads to the same local displacements as in the actual system. This effective spring constant K_e can be written in terms of a suitably generalized Watson integral for the lattice. This integral will contain all the information that is necessary to describe the rigidity of the layers and can be computed if a suitable force constant model for the layers is available. In practice the Watson integral $W(K)$ is not very sensitive to such details as can be seen from Fig. 15 which compares $W(K)$ for various lattices. Having obtained the effective spring constant K_e via the Watson integral $W(K)$, the effective-medium equations developed in Sec. IV are quite general.

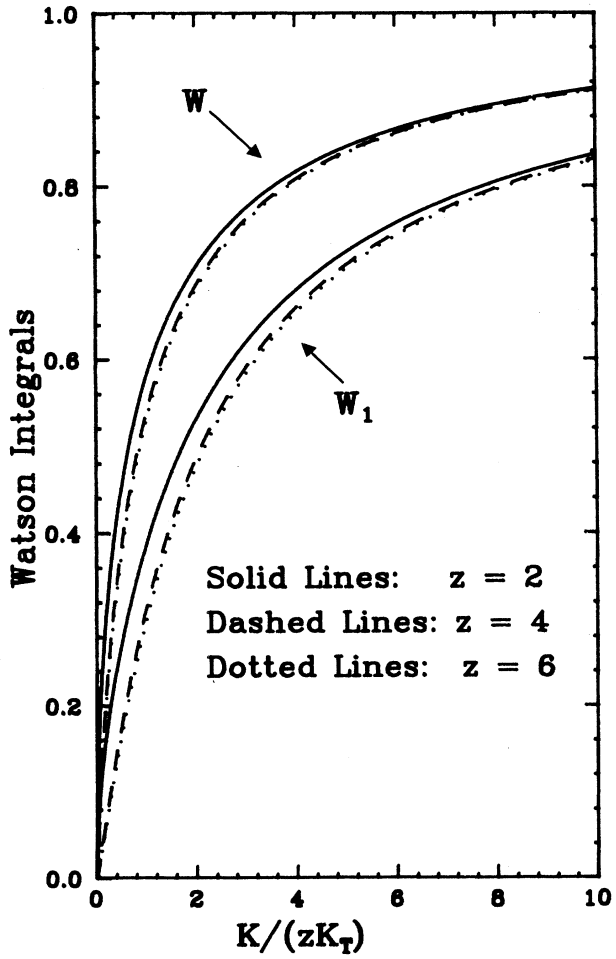

FIG. 15. The Watson integral $W(K)$ and its derivative $W_1(K)$ are shown for various lattices as a function of $K/(zK_T)$, where z is the number of nearest neighbors. Here $z=2$ is the linear chain, $z=4$ is the square net, and $z=6$ is the triangular net.

ACKNOWLEDGMENTS

We should like to thank A. R. Day and E. J. Garboczi for many interesting insights into the use of effective-medium theory for spring systems. This work was supported in part by the National Science Foundation (NSF) under Grant Nos. DMR-85-14154 and DMR-87-14865.

APPENDIX A

The Watson integrals[24] $W(K)$ used in the text are

$$W(K)=\frac{1}{N}\sum_{\vec{q}}\frac{K}{\lambda_{\vec{q}}} =\frac{a^2}{4\pi^2}\int d\vec{q}\frac{K}{K+K_T z(1-\gamma_{\vec{q}})+K_F[z(1-\gamma_{\vec{q}})]^2} \tag{A1}$$

where the $\vec{q}$ integral is over the first Brillouin whose area is $[a/(2\pi)]^2$ and the factor $\gamma_{\vec{q}}$ is given in Eq. (29). The dispersion relation for the vibrational modes is

$$\omega_{\vec{q}}^2=\{(K+K_T z(1-\gamma_{\vec{q}})+K_F[z(1-\gamma_{\vec{q}})]^2\}/m \tag{A2}$$

where m is the mass of an atom in the graphite layer. This dispersion relation corresponds to modes of vibration of the whole sample, containing many layers, in which the wave vector is in the plane and the displacements are all perpendicular to the plane. These modes could be seen, for example, in inelastic neutron scattering experiments.

It is convenient to introduce a Green function $g(x)$ defined by

$$g(x)=\frac{1}{N}\sum_{\vec{q}}\frac{K}{\lambda_{\vec{q}}}=\frac{a}{4\pi^2}\int d\vec{q}\frac{1}{x-z(1-\gamma_{\vec{q}})} \tag{A3}$$

from which can define a spectral weight $\rho(x)$ by

$$\rho(x)=-\frac{1}{\pi}\,\mathrm{Im}g(x)=\frac{1}{N}\sum_{\vec{q}}\delta(x-z(1-\gamma_{\vec{q}})) \tag{A4}$$

where x is real and $\rho(x)$ is nonzero and positive definite within the band $0<x<2z$. The Watson integral Eq. (A1) can now be written as an integral over this spectral weight:

$$W(K)=\int_0^{2z}\frac{K\rho(x)}{K+K_T x+K_F x^2}dx\ . \tag{A5}$$

The integral Eq. (A5) is well behaved as the denominator contains no poles. Note that for large $K\gg K_T, K_F$

$$W(K)\to 1 \tag{A6}$$

as we would expect. For small $K\ll K_T, K_F$ the Watson integral is dominated by the small x behavior, depends only on the ration K/K_T, and goes to zero as K goes to zero in the 1D and 2D cases of interest here.

Another related quantity $W_1(K)$ that we require can be

found directly from the Watson integral

$$W_1(K)=\frac{1}{N}\sum_{\vec{q}}\left|\frac{K}{\lambda_q}\right|^2=\int_0^{2z}\frac{K^2\rho(x)}{(K+K_Tx+K_Fx^2)^2}dx$$
$$=-K^2\frac{\partial}{\partial K}[W(K)/K]\ . \qquad \text{(A7)}$$

1. One-dimensional chain

In the case of one-dimensional chain, $z=2$ and $\gamma_q=\cos(q\delta)$, so that

$$\rho(x)=[x(4-x)]^{-1/2}/\pi \qquad \text{(A8)}$$

and the Watson integral is given by

$$W(K)=(\{1+(8K_F/K)/[1+2K_T/K+(1+4K_T/K+16K_F/K)^{1/2}]\}/(1+4K_T/K+16K_F/K))^{1/2}\ . \qquad \text{(A9)}$$

When K is small this result becomes

$$W(K)=\tfrac{1}{2}(K/K_T)^{1/2} \qquad \text{(A10)}$$

independent of K_F as discussed above. For the case when $K_F=0$, the result Eq. (A9) simplifies to

$$W(K)=(1+4K_T/K)^{-1/2} \qquad \text{(A11)}$$

and when $K_T=0$, the result Eq. (A9) becomes

$$W(K)=\{[1+(1+16K_F/K)^{1/2}]/[2(1+16K_F/K)]\}^{1/2}\ . \qquad \text{(A12)}$$

The quantity $W_1(K)$ is found by differentiation of (A9) and for $K_F=0$ is given by

$$W_1(K)=(1+2K_T/K)(1+4K_T/K)^{-3/2}\ . \qquad \text{(A13)}$$

For general values of K_F/K_T, we plot $W(K)$ in Fig. 16.

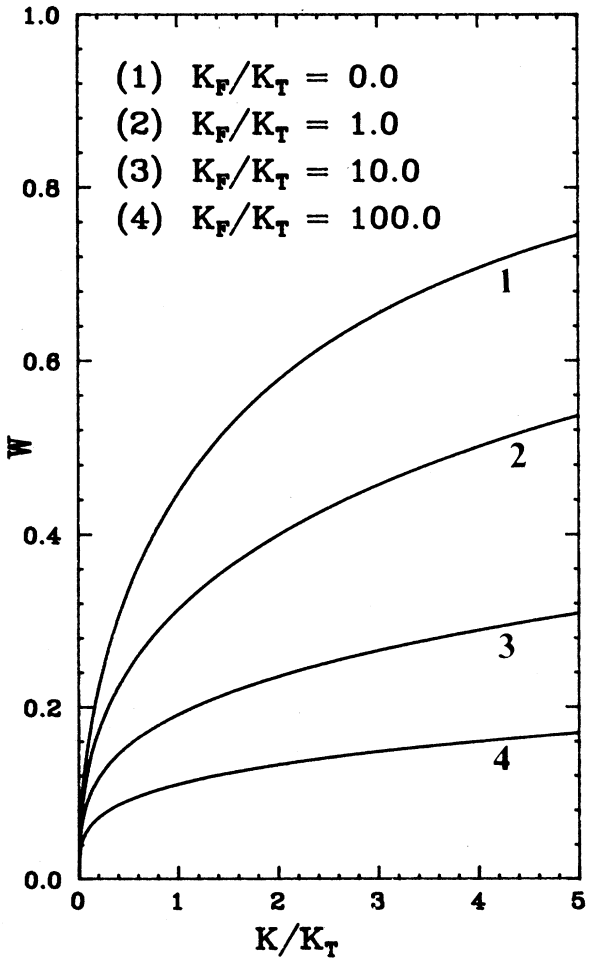

FIG. 16. The Watson integral $W(K)$ for the linear chain, for various values of K_F/K_T.

2. Square lattice

For a two-dimensional square lattice $z=4$ and

$$\gamma_{\vec{q}}=\tfrac{1}{2}[\cos(q_x\delta)+\cos(q_y\delta)]\ . \qquad \text{(A14)}$$

The spectral density can be written as an elliptic integral and leads to a density of states $\rho(x)$ given by

$$\rho(x)=\kappa\{[x(4-x)]^{1/2}/2\}/\pi^2 \qquad \text{(A15)}$$

for $0<x<4$. Here $\kappa(x)$ is the complete elliptic integral of the first kind. In general the one-dimensional integral Eq. (A5) must be done numerically. However if we put $K_F=0$, the integral can be done analytically and we obtain

$$W(K)=\frac{2}{\pi}\kappa\left[\frac{4K_T/K}{1+4K_T/K}\right]\Big/(1+4K_T/K)\ . \qquad \text{(A16)}$$

If $K_T\gg K$, the result Eq. (A16) becomes

$$W(K)=[K/(4\pi K_T)]\ln(32K_T/K)\ . \qquad \text{(A17)}$$

For $K_F=0$ we also have the result from Eqs. (A7) and (A16)

$$W_1(K)=\frac{2}{\pi}E[(4K_T/K)/(1+4K_T/K)]/(1+8K_T/K) \qquad \text{(A18)}$$

where $E(x)$ is the complete elliptic integral of the second kind.

3. Triangular lattice

For the two-dimensional triangular lattice $z=6$ and

$$\gamma_{\vec{q}}=\tfrac{1}{3}[\cos(2aq_x\delta)+2\cos(aq_x\delta)\cos(bq_y\delta)] \qquad \text{(A19)}$$

where $a=\frac{1}{2}$ and $b=\sqrt{3}/2$. Carrying out the integral for the spectral weight we obtain

$$g(x)=\frac{1}{\pi^2}\int_0^\pi dx\int_0^\pi dy\frac{1}{x-z[1-\frac{1}{3}(\cos 2x+2\cos x\cos y)]}\ , \tag{A20}$$

leading to

$$\rho(x)=\frac{1}{2\pi}(x-3)^{-1/4}\kappa[(1-s)^{1/2}] \tag{A21}$$

where

$$s=\frac{[(x-3)^{1/2}-1]^3[(x-3)^{1/2}+3]}{16(x-3)^{1/2}}\ .$$

In general the Watson integral Eq. (A5) must be done numerically over the spectral weight. If $K_F=0$, it can be done analytically to give

$$W(K)=\frac{K}{4\pi K_T}g\kappa[(g/2)(9+K/K_T)^{1/4}] \tag{A22}$$

where

$$g=\frac{8}{[(9+K/K_T)^{1/2}-1]^{3/2}[(9+K/K_T)^{1/2}+3]^{1/2}}\ .$$

If $K_T\gg K$, the result Eq. (A22) becomes

$$W(K)=[K/(4\pi K_T\sqrt{3})]\ln(72K_T/K)\ . \tag{A23}$$

The quantity $W_1(K)$ can be found by differentiation.

APPENDIX B

In this appendix, we show that the effective-medium solution is not exact. At some stage we thought that it might be exact, because it reproduced all the known exact results and agreed extremely well with our numerical simulations. However, this is not the case as can be seen by the following counterexample.

We consider a one-dimensional chain, with $K_F=0$ and with $K_A=\infty$. In this limit the effective medium Eq. (34) for a linear chain becomes

$$(1-x)(1+4K_T/K)^{1/2}=1-K_B/K\ . \tag{B1}$$

Solving this for K and expanding the dimensionless height to second order in x, we find that

$$\langle d\rangle=xK_B/(K_B+2K_T)\times[1+2xK_T(K_B+3K_T)/(K_B+2K)^2+\cdots]\ . \tag{B2}$$

The exact expression can be developed as a power series in x. The first term comes from a single defect. The rest of the lattice is frozen with $d_i=0$ because of the infinite spring constant K_A. The d of the defect site can be found by minimizing the energy with respect to d to give $K_B/(K_B+2K_T)$. For two adjacent defects, both have the same d, so that minimizing the energy for the pair with respect to d leads to $K_B/(K_B+K_T)$. Thus the exact $\langle d\rangle$ to second order in x is

$$\langle d\rangle=x(1-x)^2K_B/(K_B+2K_T)+2x^2(1-x)^2K_B/(K_B+K_T)+\cdots\ , \tag{B3}$$

which leads to

$$\langle d\rangle=xK_B/(K_B+2K_T)[1+2xK_T/(K_B+K_T)+\cdots]\ , \tag{B4}$$

which demonstrates that the effective-medium result Eq. (B2) is different from the exact result Eq. (B4) in the pair terms involving x^2.

[1]F. S. Galasso, *Structure and Properties of Inorganic Solids* (Pergamon, New York, 1970).
[2]L. Vegard, Z. Phys. **5**, 17 (1921).
[3]J. B. Thompson, in *Researches in Geochemistry*, edited by P. H. Abelson (Wiley, New York, 1967), Vol. II, p. 340.
[4]J. R. Dahn, D. C. Dahn, and R. R. Haering, Solid State Commun. **42**, 179 (1982).
[5]J. E. Fisher and H. J. Kim, Phys. Rev. B **35**, 3295 (1987).
[6]S. A. Solin and H. Zabel, Adv. Phys. **37**, 87 (1988).
[7]P. C. Chow and H. Zabel, Phys. Rev. B **38**, 12 837 (1988).
[8]D. Medjahed, R. Merlin, and R. Clarke, Phys. Rev. B **36**, 9345 (1987).
[9]W. Jin and S. D. Mahanti, Phys. Rev. B **37**, 8647 (1988).
[10]H. Kim, W. Jin, S. Lee, P. Zhou, T. J. Pinnavaia, S. D. Mahanti, and S. A. Solin, Phys. Rev. Lett. **60**, 2168 (1988); S. Lee, S. A. Solin, W. Jin, and S. D. Mahanti, in *Graphite Intercalation Compounds: Science and Applications,* Proceedings of the MRS 1988 Meeting, Boston, edited by M. Endoh, M. S. Dresselhaus, and G. Dresselhaus (Materials Research Society, Pittsburgh, 1988), p. 41.
[11]M. F. Thorpe, Phys. Rev. B **39**, 10 370 (1989).
[12]S. Lee, H. Miyazaki, S. D. Mahanti, and S. A. Solin, Phys. Rev. Lett. **62**, 3066 (1989).
[13]H. Miyazaki, S. Lee, S. D. Mahanti, and S. A. Solin (unpublished).
[14]K. Komatsu, J. Phys. Soc. Jpn **6**, 438 (1951).
[15]M. F. Thorpe (unpublished).
[16]S. Feng, M. F. Thorpe, and E. Garboczi, Phys. Rev. B **31**, 276 (1985).
[17]R. P. Feynman, Phys. Rev. **56**, 340 (1939).

[18]R. Fletcher, *Practical Methods of Optimization* (Wiley, New York, 1980); J. Stoer and R. Bulirsch, *Introduction to Numerical Analysis* (Springer-Verlag, New York 1980), p. 572.

[19]W. M. Press, B. P. Flannery, S. A. Teukolsky, and W. T. Vetterling, *Numerical Recipes* (Cambridge University Press, Cambridge, England, 1986), p. 301.

[20]H. Zabel (private communication); W. Krone, G. Worthmann, G. Kaindl, and H. Zabel [in Proceedings of the 5th International Symposium on Graphite Intercalation Compounds, Berlin, 21–24 May (1989)] have reported some preliminary EXAFS measurments in $K_{0.52}Rb_{0.48}C_8$, but they have not made a systematic probe of $\langle d_K \rangle$ and $\langle d_{Rb} \rangle$ as functions of x (unpublished).

[21]F. DiSalvo (private communication).

[22]J. C. Mikkelsen, Jr. and J. B. Boyce, Phys. Rev. B **28**, 7130 (1983).

[23]M. F. Thorpe (unpublished).

[24]G. N. Watson, Q. J. Math (Oxford) **10**, 266 (1939); T. Horiguchi, J. Math. Phys. **13**, 1411 (1972).